

# UC Irvine

## UC Irvine Previously Published Works

### Title

Human neural stem cell-derived extracellular vesicles mitigate hallmarks of Alzheimer's disease

### Permalink

<https://escholarship.org/uc/item/13s3t6g6>

### Journal

Alzheimer's Research & Therapy, 13(1)

### ISSN

1758-9193

### Authors

Apodaca, Lauren A  
Baddour, Al Anoud D  
Garcia, Camilo  
[et al.](#)

### Publication Date

2021

### DOI

10.1186/s13195-021-00791-x

### Copyright Information

This work is made available under the terms of a Creative Commons Attribution License, available at <https://creativecommons.org/licenses/by/4.0/>


Peer reviewed

RESEARCH

Open Access



# Human neural stem cell-derived extracellular vesicles mitigate hallmarks of Alzheimer's disease

Lauren A. Apodaca<sup>1</sup>, Al Anoud D. Baddour<sup>1</sup>, Camilo Garcia Jr<sup>1</sup>, Leila Alikhani<sup>1</sup>, Erich Giedzinski<sup>1</sup>, Ning Ru<sup>1</sup>, Anshu Agrawal<sup>2</sup>, Munjal M. Acharya<sup>1\*</sup> and Janet E. Baulch<sup>1\*</sup> 

## Abstract

**Background:** Regenerative therapies to mitigate Alzheimer's disease (AD) neuropathology have shown very limited success. In the recent era, extracellular vesicles (EVs) derived from multipotent and pluripotent stem cells have shown considerable promise for the treatment of dementia and many neurodegenerative conditions.

**Methods:** Using the 5xFAD accelerated transgenic mouse model of AD, we now show the regenerative potential of human neural stem cell (hNSC)-derived EVs on the neurocognitive and neuropathologic hallmarks in the AD brain. Two- or 6-month-old 5xFAD mice received single or two intra-venous (retro-orbital vein, RO) injections of hNSC-derived EVs, respectively.

**Results:** RO treatment using hNSC-derived EVs restored fear extinction memory consolidation and reduced anxiety-related behaviors 4–6 weeks post-injection. EV treatment also significantly reduced dense core amyloid-beta plaque accumulation and microglial activation in both age groups. These results correlated with partial restoration of homeostatic levels of circulating pro-inflammatory cytokines in the AD mice. Importantly, EV treatment protected against synaptic loss in the AD brain that paralleled improved cognition. MiRNA analysis of the EV cargo revealed promising candidates targeting neuroinflammation and synaptic function.

**Conclusions:** Collectively, these data demonstrate the neuroprotective effects of systemic administration of stem cell-derived EVs for remediation of behavioral and molecular AD neuropathologies.

**Keywords:** Alzheimer's disease, Extracellular vesicle, Neural stem cell, Inflammatory response

## Background

The most common form of dementia is Alzheimer's disease (AD), an irreversible neurodegenerative disease that is characterized by progressive cognitive and functional decline and memory loss [1]. Currently, there are no effective therapies to slow or reverse the disease progression. Hallmarks of AD include amyloid-beta (A $\beta$ ) plaques, neurofibrillary tangles, and neuroinflammation

which is accompanied by dementia. Microglia, the resident macrophages of the brain, become activated to engulf and clear the extracellular A $\beta$  plaque deposits. However, persistent microglial activation in AD eventually leads to a pro-inflammatory environment that includes increased expression of pro-inflammatory cytokines and reduced expression of anti-inflammatory cytokines [2–4]. Ultimately, this chronic inflammation, in addition to the plaque deposition, creates a neurotoxic microenvironment that leads to loss of dendritic spines and neurons in the AD brain [4].

\* Correspondence: [macharya@uci.edu](mailto:macharya@uci.edu); [jbaulch@uci.edu](mailto:jbaulch@uci.edu)

<sup>1</sup>Department of Radiation Oncology, University of California Irvine, Irvine, CA 92697, USA

Full list of author information is available at the end of the article



© The Author(s). 2021 **Open Access** This article is licensed under a Creative Commons Attribution 4.0 International License, which permits use, sharing, adaptation, distribution and reproduction in any medium or format, as long as you give appropriate credit to the original author(s) and the source, provide a link to the Creative Commons licence, and indicate if changes were made. The images or other third party material in this article are included in the article's Creative Commons licence, unless indicated otherwise in a credit line to the material. If material is not included in the article's Creative Commons licence and your intended use is not permitted by statutory regulation or exceeds the permitted use, you will need to obtain permission directly from the copyright holder. To view a copy of this licence, visit <http://creativecommons.org/licenses/by/4.0/>. The Creative Commons Public Domain Dedication waiver (<http://creativecommons.org/publicdomain/zero/1.0/>) applies to the data made available in this article, unless otherwise stated in a credit line to the data.

Similar neuropathologies including persistent inflammation, loss of synaptic integrity, and cognitive impairments have been clearly shown to manifest in the radiation-damaged brain [5]. In a series of studies, we demonstrated that hippocampal engraftment of human neural stem cell (hNSC) ameliorated neurocognitive and neuroinflammatory effects of a clinically relevant radiation exposure using athymic nude rats [6–9]. These studies showed that stem cell-based approaches improved the functional plasticity of the irradiated host brain, suppressing neuroinflammation, preserving host neuronal morphology, and improving cognitive function. Since significant attrition of engrafted cells was observed, it was hypothesized that the hNSC provided neuroprotective benefits primarily via trophic support rather than proliferation and repopulation [10–12].

A somewhat similar trajectory involving stem cells has been observed in the search for effective approaches to ameliorate AD neuropathology. Studies have demonstrated that hNSC transplantation can provide at least some neurocognitive benefits in transgenic mouse models of AD [13]. The data from both radiation and AD studies have suggested that the neuroprotective properties and trophic support mechanisms by which NSC act to reduce inflammation and preserve the structural integrity of the injured brain are via the stem cell secretome, more specifically stem cell-derived extracellular vesicles (EVs) [10–12, 14, 15]. In the case of cranial irradiation, this assertion has been borne out through a series of studies, using hNSC-derived EVs. In a first study, the efficacy of EV therapy was demonstrated in an irradiated athymic nude rat model [10, 12] and then in a study using immunocompetent mice [11]. Studies by others have similarly indicated that mouse stem cell-derived EV transplantation can provide neurocognitive benefits in transgenic mouse models of AD [14, 15].

EVs are small membrane-bound vesicles that are less immunoreactive than their cellular source and contain bioactive cargo such as proteins, mRNA, and microRNA (miRNA) [16]. Endogenously, EVs are recognized as important modulators of physiological processes, with specific cargo capable of controlling cell signaling and target cell function to maintain homeostasis or to contribute to disease pathology [17–19]. Exogenous stem cell-derived EVs represent a unique paracrine signaling mechanism with great therapeutic potential, particularly in the context of CNS injuries such as traumatic brain injury, stroke, and neurodegenerative diseases [14, 15, 19–22]. These EVs not only cross the blood-brain barrier but also negate concerns regarding the possibility of teratoma formation and immune rejection that confound related stem cell-based approaches [23–25]. Immune rejection is a particularly significant problem in the case of AD, since the long-term use of immunosuppressant can

result in toxicity, particularly in the aged, and may also exacerbate AD-related pathologies [22, 26].

In this study, the 5xFAD mouse model of AD that co-expresses five human familial AD mutations was used [27]. The 5xFAD mouse is an accelerated model of AD with measurable A $\beta$  plaque load by 2 months of age but in the absence of neurofibrillary tangles. These animals also exhibit reductions in synaptophysin, neuronal loss, and memory impairments that become evident by 5–6 months of age. The goal of this study was to test the hypothesis that hNSC-derived EV treatment could mitigate AD-related behavioral and molecular neuropathologies when delivered intravenously to early- or late-stage AD mice.

## Materials and methods

### hNSC culture and EV isolation and characterization

The use of hNSC was approved by the Institutional Human Stem Cell Research Oversight Committee (HSCRO). The validation, expansion, and characterization of hNSC (ENStem-A; EMD Millipore) followed previously published procedures [28]. Before isolation of extracellular vesicles (EVs), the conditioned hNSC culture medium was put through a 0.22- $\mu$ m sterile filter as an initial purification step before centrifugation. EVs were then isolated and further purified from the hNSC culture medium by ultracentrifugation [10, 29] and characterized for size and number by a ZetaView particle analyzer as per instrument instructions (ZetaView PMX 110; Meerbusch, Germany).

EVs were also analyzed by electron microscopy for morphology where the material was negatively stained by applying a drop of EV solution (final concentration approximately 1 mg/ml) directly onto a 300-mesh formvar-carbon-coated nickel grid (Electron Microscopy Sciences; Hatfield, PA), which was allowed to remain for approximately 60 s, after which excess solution was removed. A drop of 1% aqueous uranyl acetate was then added onto the grid and allowed to remain for an additional 60 s, after which excess solution was removed and the grids allowed to dry. Material was imaged on a Hitachi 7500 transmission electron microscope equipped with an Advanced Imaging Technologies (AMT) digital camera. A digital point-to-point measuring tool (AMT) was used to determine exosome size distribution. Images were imported into Photoshop CS2 (Adobe Systems Inc.) where they were sized and optimized for contrast and brightness.

### Animals and EV delivery

All animal experimentation procedures were performed under the guidelines provided by NIH and approved by the University of California Irvine Institutional Animal Care and Use Committee. Male 5xFAD transgenic mice

and age-matched littermate controls were maintained in standard housing conditions ( $20^{\circ}\text{C} \pm 1^{\circ}\text{C}$ ;  $70\% \pm 10\%$  humidity; 12-h:12-h light and dark cycle) and provided ad libitum access to standard rodent chow (Envigo Teklad 2020x) and water. For the early-stage AD study, male 5xFAD mice and their wild type littermate controls were divided into the following groups: vehicle-injected AD with sterile hibernation buffer (Gibco) (AD;  $N = 15$ ), EV-injected AD (AD+EV;  $N = 16$ ), and vehicle-injected wild type (WT;  $N = 16$ ). The mice were 1.5–2.5 months of age at the time of EV treatment and stratified by age to maintain equivalent age distributions among experimental groups. Behavior studies were initiated 1-month post-EV treatment when mice were 2.5–3.5 months of age. The late AD study utilized the same treatments and stratification of male mice where the AD mice and their WT littermate controls were 5.0–6.5 months of age ( $N = 14$ –16 AD, AD+EV, WT) at the first EV treatment. A second EV injection was administered 2 weeks later. One month after the second EV treatment, when the mice reached 6.5–8.0 months of age, behavior studies were initiated.

Our previous published studies demonstrated equal effectiveness of EV treatment using both intra-hippocampal stereotaxic surgery and injection into the retro-orbital sinus (RO) [11]. Therefore, the relatively non-invasive RO injection route of EV administration was used in this study. To administer EVs, mice were sedated using 2.5% (v/v) isoflurane/oxygen, and  $2.25 \times 10^7$  EVs in 50  $\mu\text{l}$  hibernation buffer were delivered into circulation via RO injection. Control AD and WT mice received RO injections on that same schedule using 50  $\mu\text{l}$  of vehicle. Over the years, our group, and others, have not included grafted controls (either stem cells or EVs) since such transplantation procedures used to treat a variety of pathologies in different rodent models were not found to functionally affect the intact normal brain [10, 30–33]. Importantly, our past work using stem cells [34] and from others using EVs [35, 36], in which grafted controls were included, found that all functional and molecular endpoints were statistically indistinguishable between the control, stem cell-treated control, or EV-treated control groups. Further rationale for excluding controls treated with EVs alone is that inclusion of such cohorts is clinically irrelevant.

### Behavioral testing

Behavioral studies began 1 month after EV treatment using  $N = 15$ –16 mice per group as described above. Testing occurred over 3 weeks and included the following paradigms in order: novel object recognition (NOR), elevated plus maze (EPM), light-dark box (LDB), and fear extinction (FE) memory tasks. Independent investigators blinded to the experimental groups scored all

behavior videos. NOR, EPM, and LDB were scored manually, while FE was scored for freezing using Freeze-Frame (Coulbourn Instruments). See [Supplemental Information](#) for details.

The spontaneous exploration task NOR relies on intact hippocampal, medial prefrontal cortex (mPFC), and perirhinal cortex (PRC) function, evaluating episodic recognition memory by measuring the preference of mice to investigate novelty [37, 38]. Mice were habituated to the arena with only bedding for 3 days followed by a test day where mice were presented with two plastic objects that were similar in color, shape, and size. Each mouse was returned to the home cage for 5 min while one familiar object was substituted for a novel object. The mouse was then returned to the arena for 5 min of further exploration. The discrimination index, as measured by the time spent interacting with familiar versus novel objects, was then calculated for each mouse from these values:  $[(\text{novel}/\text{total exploration time}) - (\text{familiar}/\text{total exploration time})] \times 100$ .

The EPM and LDB tests are based on the tendency of anxious rodents to avoid open or brightly lit areas and to exhibit reluctance to explore open environments, resulting in reduced amounts of time spent in the open arms of the EPM or reduced numbers of transitions between the dark and light compartments of the LDB testing arena [39]. The EPM consists of 2 open arms and 2 closed arms arranged in the shape of a plus sign [40, 41]. Each mouse was placed in the neutral center zone of the plus maze and allowed to explore for 5 min. Anxiety-like behavior was scored as the percent time spent in the open arms of the maze as compared to the closed arms. Following EPM, the next day, mice were tested on LDB where anxiety was measured by a mouse's willingness to transition freely between a large well-lit chamber to a smaller, dimly lit chamber. Fewer transitions and less time spent in the well-lit chamber during the 10-min test suggested increased anxiety-like behavior [39].

The last behavior test administered was the FE test where two contexts (A and B) were used to determine whether mice could learn and then extinguish conditioned fear responses over 5 days [42, 43]. The conditioning testing chamber (context A) had a steel grid floor and the scent of acetic acid, while the extinction chamber (context B) had a smooth Plexiglas floor, additional stimulus lighting, and the scent of almond extract. Freezing behavior was recorded via digital cameras mounted in the ceiling of each chamber automated scoring (FreezeFrame, Coulbourn Instruments). For each mouse, the fear conditioning protocol for day 1 used context A and started with a 120-s habituation phase followed by 3 pairings of a 120-s white noise conditioned stimulus (CS) co-terminating with a 1-s foot shock (US) presented at 2-min intervals (day 1,  $T_1$ – $T_3$ ). For

extinction training, starting on day 2, each mouse was placed in context B and allowed to acclimate for 2 min followed by extinction training that was comprised of 15 non-reinforced 120-s CS presentations presented graphically as the average of 5 tones. Extinction training was repeated daily for 2 additional days. Subsequently, retention testing was performed on day 5 where each mouse was returned to context B and following a 2-min acclimation period freezing was assessed during three non-US-reinforced CS tones at 2-min intervals. Extinction memory was calculated as the percentage of time spent freezing during the test.

#### **Thioflavin-S (Thio-S) staining, immunohistochemistry, and confocal microscopy analysis**

Following behavior, a subset of those same mice was deeply anesthetized using isoflurane and euthanized via intracardiac perfusion using 4% paraformaldehyde (Sigma) in 100 mM phosphate-buffered saline (PBS; pH 7.4, ThermoFisher Scientific). Brains were cryoprotected (10–30% sucrose gradient over 2–3 days) and sectioned coronally into 30  $\mu\text{m}$  using a cryostat (Leica Microsystems, Germany). For each endpoint, 4 representative coronal brain sections of the amygdala and medial prefrontal cortex (mPFC) regions from each of the 4 animals per experimental group were selected at approximately 15 section intervals, washed in PBS, and stored in PBS. Sections were rehydrated in ethanol gradients (100%, 95%, 70%, 50%) and then incubated in a 0.5% Thio-S solution in 50% ethanol for 10 min. Tissues were rinsed twice in 50% ethanol and then rinsed twice in PBS. Sections were mounted and sealed with slow fade/gold antifade mounting medium (Life Technologies). Confocal imaging was conducted using Nikon Eclipse Ti C2 microscope (Nikon, Japan) equipped with a 20 $\times$  lens and NIS-Elements AR interface (v4.30, Nikon). Approximately, 20–25 z stacks (1  $\mu\text{m}$  thick) were collected that were uploaded to AutoQuant deconvolution module (version X3.0.4, Media Cybernetics, Rockville, MD) followed by direct recall into the Imaris module (version 8.1.2, Bitplane, Inc., Zurich, Switzerland) to create surface reconstruction of the deconvoluted, Thio-S-positive (green) surfaces. The number of Thio-S-positive plaques per section was reported to determine the extent of plaque deposition in each group.

Immunohistochemistry was also performed on the PFA-fixed brain sections. For the immunofluorescence labeling of microglial activation marker CD68 and pre-synaptic marker synaptophysin, rat anti-mouse CD68 (1:500; AbD Serotec) and mouse-anti-synaptophysin (1:1000, Sigma) primary antibodies, respectively, were used with Alexa Fluor 568 secondary antibody (1:500 and 1:1000, respectively). Tissues were then DAPI nuclear

counterstained and sealed in slow fade/gold antifade mounting medium (Life Technologies).

The stained coronal brain sections were scanned using a confocal microscope (Nikon Eclipse Ti C2) equipped with a 40 $\times$  PlanApo oil-immersion lens (1.3 NA, Nikon) and an NIS-Elements AR interface (v4.30, Nikon). Thirty z stacks (1024 bit depth) at 0.5  $\mu\text{m}$  from three different fields (318  $\times$  318  $\times$  24  $\mu\text{m}$ ) were imaged in each section in the areas of interest. The digitized z stacks were deconvoluted using the AutoQuant software. An adaptive, 3D blinded method was used to create deconvoluted images for direct import into the Imaris module. The 3D algorithm-based surface rendering and quantification of fluorescence intensity for each fluorescently labeled marker was carried out in Imaris at 100% rendering quality. Each channel was analyzed separately. 3D surface rendering detects immunostained puncta or nuclear staining (DAPI) satisfying pre-defined criteria, for the puncta size (0.5 to 1  $\mu\text{m}$ ) verified visually for accuracy. Using deconvoluted confocal z stack volume from the control group (WT) as a baseline for the minimum thresholding, a channel mean intensity filter was applied and used for all the experimental groups for each batch of molecular markers. The pre-set parameters were kept constant throughout the subsequent analysis of immunoreactivity for each antigen. To maintain uniformity among the varying number of puncta for each time point and/or antigen analyzed, the number of puncta per 318  $\times$  318  $\times$  24  $\mu\text{m}$  was normalized to WT control, and data was expressed as percent mean immunoreactivity relative to WT controls.

#### **Amyloid- $\beta$ ELISA**

Fresh frozen brain tissues were isolated from another subset of the behaviorally tested mice. As per the manufacturer's protocol, isolated protein samples from fresh frozen brains were applied to a blocked MSD Human/Rodent (4G8) A $\beta$  triplex ELISA plate and incubated for 2 h at room temperature on an orbital shaker (A $\beta_{1-38}$ , A $\beta_{1-40}$ , A $\beta_{1-42}$ ; Meso Scale Discovery, Rockville MD). The plate was then washed, and measurements obtained using a SECTOR Imager 2400.  $N=7$  and 6 mice per experimental group for AD and AD+EV soluble A $\beta$  measurements and  $N=7$  mice per experimental group for insoluble A $\beta$  measurements, with 1 WT negative control for both measurements.

#### **Spleen cytokine analysis and flow cytometry**

Fresh spleens were collected from early- and late-stage AD, AD+EV, and WT mice, 7 mice per group. For cytokine analysis, spleen cells ( $1 \times 10^6/\text{ml}$ ) were stimulated with phorbol 12-myristate 13-acetate (PMA; 50 ng/ml; Sigma) and ionomycin (1  $\mu\text{g}/\text{ml}$ ; Sigma) in RPMI medium containing 10% FBS. Supernatants collected

after overnight stimulation were assayed for IFN- $\gamma$ , IL-17, and IL-10, IL-1 $\beta$ , using a magnetic bead-based kit (Thermo Fisher Scientific). Single-cell spleen suspensions were stained with antibodies specific to B1 cells (CD19<sup>+</sup>CD5<sup>+</sup>CD43<sup>+</sup>; Biolegend, San Diego, CA). The analysis was done using Flow Jo software (Treestar, Ashland, OR).

#### Gene expression analysis

Total mRNA was purified from the fresh frozen hippocampus of each of 4 mice per group, WT, AD, and AD+EV, from the late-stage AD cohort and multiplexed using the nCounter Mouse Neuroinflammation Panel that includes 757 genes that cover core pathways that define neuroinflammation processes and 13 internal reference genes (NanoString, CA).

Counts for target genes were normalized to the housekeeping genes to account for variability in RNA content. Background signal was calculated as a mean value of the negative hybridization control probes. Gene expression values were presented as the percentage of the WT control group for comparison of the AD cohort to the AD+EV cohort.

#### MicroRNA microarray and validation

The hNSC-derived EVs were lysed using Qiazol and miRNA isolated using the Qiagen miRNeasy kit as per the manufacturer's protocol (Qiagen, CA). Samples were analyzed for integrity and concentration (NanoDrop; 260/280 ratio > 1.6 and 260/230 ratio > 1.5), then processed and analyzed in duplicate on a miRNA microarray chip (Exiqon, Denmark; Genomics Shared Resource at the University of Texas South Western Medical Center). Results were delivered as a spreadsheet of miRNA IDs and their associated expression values. Negative control probes were included for the determination of significant hits. Another spreadsheet provided was filtered for probes that had duplicate measurements with less than 15% coefficient of variation (CV) and at least three standard deviations greater than the negative control probes.

Select candidate miRNA from the array were identified through literature searches of miRNA implicated in AD pathologies. Validation of those candidate miRNAs was performed using TaqMan Advanced miRNA Assays (ThermoFisher, MA). Total RNA was extracted from two independent EV preparations using the RNA mini-prep kit (Zymo Research Corp., CA). RNA template was then ligated to adaptors and pre-amplified using the TaqMan Advanced miRNA cDNA Synthesis Kit (ThermoFisher) as per the manufacturer's protocol to obtain the cDNA template for classical qPCR using specific TaqMan Advanced miRNA Assays (ThermoFisher) which are primers specific to the target miRNA.

Duplicate reactions were set up in a 96-well plate with no-template controls (MilliQ water instead of total RNA was used for cDNA synthesis process) included for each assay. Cycling was performed in the CFX96 (BioRad Laboratories, Inc., CA). qPCR data were visualized and processed using CFX Manager software (BioRad Laboratories, Inc., CA).

#### Statistical analysis

Statistical analyses were carried out using GraphPad Prism (v6). The Shapiro-Wilk test was used to assess the normal distribution of all behavioral testing data. Unless stated otherwise, one-way analysis of variance (ANOVA) was used to assess the significance for the AD, AD+EV, and WT groups of mice. When overall group effects were found to be statistically significant, Bonferroni's multiple comparisons test was used to compare the AD group with each of the other experimental groups. A *P* value of  $\leq 0.05$  was considered to be statistically significant.

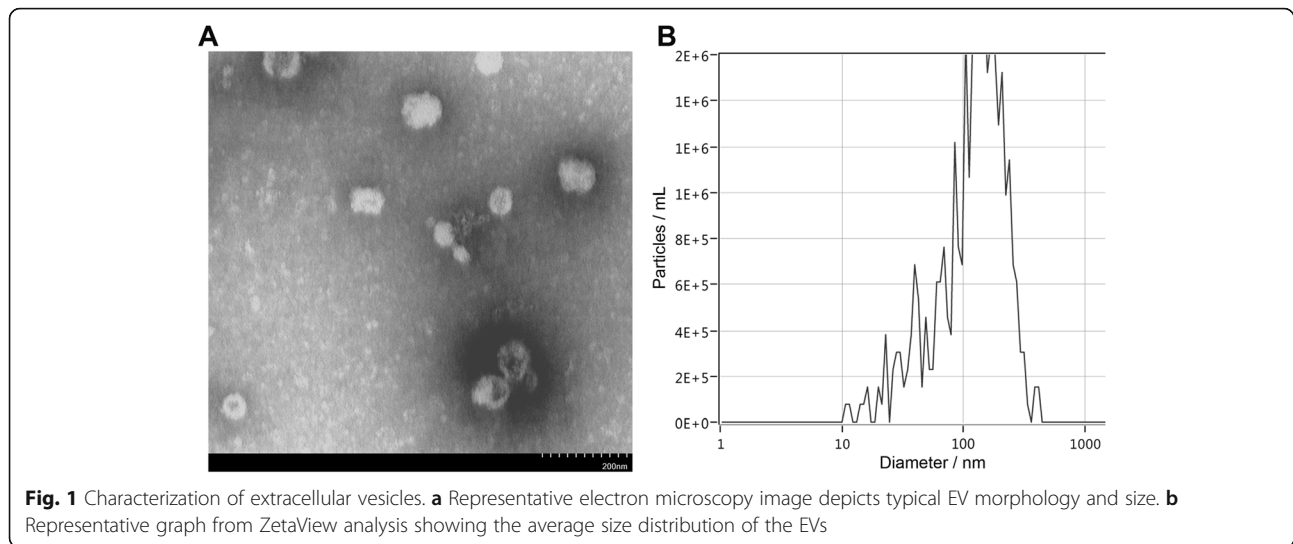
## Results

#### EV characterization and experimental design

EVs were characterized for morphology by electron microscopy and for size and number using a ZetaView particle analyzer. The mean EV size was  $147.8 \pm 2.1$  nm diameter at a mean stock concentration of  $7.58 \times 10^9 \pm 6.40 \times 10^8$  EV per ml (Fig. 1). The purified EVs were diluted into sterile hibernation buffer to deliver  $2.25 \times 10^7$  EV per 50  $\mu$ l RO injection. For the early-stage AD study, male 5xFAD mice and their wild type littermate controls were 1.5–2.5 months of age at the time of EV treatment and behavior studies were initiated 1-month post-EV treatment when mice were 2.5–3.5 months of age. The late AD study utilized the same treatments and stratification of male mice where the AD mice and their WT littermate controls were 5.0–6.5 months of age at the first EV treatment. A second EV injection was administered 2 weeks later. One month after the second EV treatment, when the mice reached 6.5–8.0 months of age, behavior studies were initiated (Fig. 2).

#### Effects of disease progression and EV treatment on cognitive function

One month after RO injection of EVs, the mice were habituated and tested on the NOR task that engages hippocampal and medial prefrontal cortex (mPFC) function [37, 38] that may be impaired in AD. For this task, the total exploration time during the familiarization phase for each object was not different between any of the experimental groups for either the early or the late AD studies, suggesting that there were no AD-related alterations in locomotion or exploratory behavior (Supplemental Table 1). While there were no significant

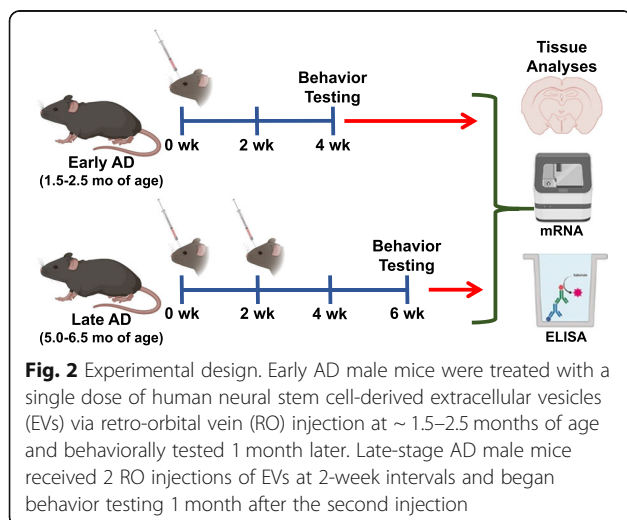


differences between WT, AD, and AD+EV mice during the test phase of the NOR task for either the early or late AD studies, there was a trend for decreased novel object exploration in the AD mice as compared to both WT and AD+EV cohorts of late AD mice (Fig. 3a and d, respectively).

Because altered mood frequently manifests in AD [44], we also used the EPM and LDB tests as a measure of anxiety-like behavior. Early AD male mice spent significantly less time in the open arms of the maze as compared to both WT and AD+EV mice ( $P < 0.05$ ), suggesting increased AD-related anxiety that could be ameliorated at early disease times by a single EV treatment (Fig. 3b). However, these mice did not exhibit any reluctance to transition between light and dark

compartments during LDB testing (Fig. 3c). Conversely, the late AD males exhibited no anxiety-like behavior on the EPM (Fig. 3e) but did show fewer transitions between compartments on the LDB test that were again mitigated by EV treatment ( $P < 0.01$ ; Fig. 3f).

AD mice can successfully learn the aversive association during the conditioning phase of the FE test but are impaired in dissociative learning [45]; thus, we evaluated the extinction of fear memory, the active process of memory consolidation [46]. Indeed, during the fear acquisition phase of testing, all mice from both the early and late AD cohorts showed similar percent times freezing during the 3 tone-shock pairings (Fig. 4a, c; T1–3 conditioning). During the subsequent fear extinction training in a new context, early WT and AD+EV mice demonstrated gradual decreases in freezing behavior over the day 2 and day 3 trials as compared to the AD mice that continued to freeze at a significantly higher level (Fig. 4a; day 1–3 extinction training). The results of the final day of extinction testing showed that the WT and AD+EV mice had equivalent fear extinction as illustrated by reduced percent times freezing as compared to the AD mice that continued to freeze for a significant percentage of the test time (Fig. 4b;  $P < 0.05$ ). This AD-related impairment of fear memory extinction suggests dysfunction of neural circuitry in the hippocampus, mPFC, and amygdala [26, 45] that could be ameliorated by EV treatment. While not statistically robust, similar trends were seen in the late AD study (Fig. 4c, d).



### Stem cell-derived EVs reduce A $\beta$ plaques in the AD brain

To determine whether EV treatment reduced amyloid pathology observed in AD, we stained for dense core plaques using Thio-S. In the early-stage AD mice that

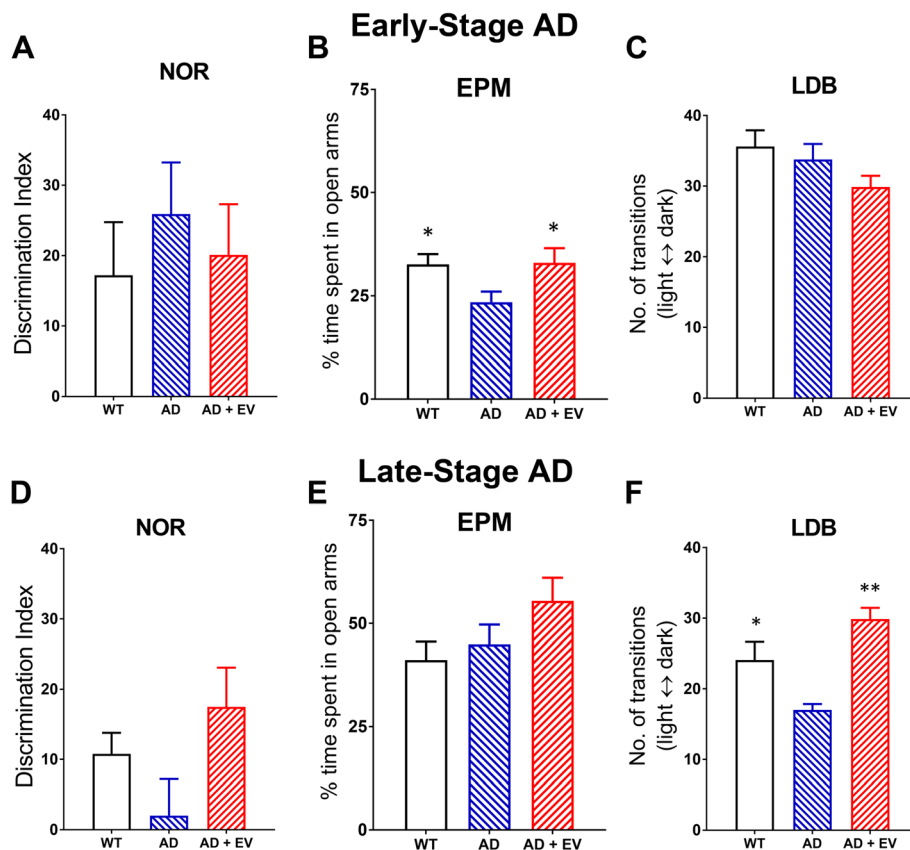


**Fig. 3 a–c** Early-stage AD behavioral testing indicated no impairments on novel object recognition (NOR) or light-dark box (LDB) tests, but AD mice showed increased anxiety-like behavior on the elevated plus maze (EPM) test that was mitigated by EV treatment. **d–f** Late-stage AD mice exhibited no significant impairments on NOR or EPM tests, but increased anxiety-like behavior on the LDB test that was mitigated by EV treatment as shown by an increased number of transitions between the light-dark compartments. Data are presented as mean  $\pm$  SEM where  $N = 14$ – $16$  mice/group.  $P$  values are derived from ANOVA and Bonferroni's multiple comparisons test. \* $P < 0.05$ , \*\* $P < 0.01$  as compared to AD

underwent EV treatment at  $\sim 2$  months of age, the plaque load was still very low. Nonetheless, EV treatment reduced the number of plaques in the infralimbic and prelimbic areas of the mPFC (Fig. 5a;  $P < 0.05$  compared to AD). In the late-stage AD mice that received EV treatment starting at 5.0–6.5 months of age, where the plaque load was significantly higher, EV treatment significantly reduced the number of A $\beta$  plaques in both the amygdala (Fig. 5b–d;  $P < 0.01$ ) and the mPFC (Fig. 5b, e, f;  $P < 0.005$ ) regions of the brain. We then evaluated the levels of both soluble and insoluble A $\beta_{1-42}$ , A $\beta_{1-40}$ , and A $\beta_{1-38}$  in the brain using triplex ELISA. While no difference between groups was observed for soluble A $\beta_{1-42}$  and A $\beta_{1-38}$ , A $\beta_{1-40}$  levels were significantly reduced in the brains of late-stage AD mice that had received EV treatment (Fig. 5g;  $P < 0.05$ ). No differences were observed between AD and AD+EV mice for any species of insoluble A $\beta$  (Fig. 5h). Together, these data suggest that just one to two EV treatments can

contribute to either reduced production of A $\beta$  or aid in clearance.

#### Effect of EV treatment on activated microglia

Microglia, the innate immune cells of the CNS, have a protective function in modulating the accumulation of A $\beta$  plaques in the early stages of AD. However, evidence suggests that once activated, the microglia become a source of damaging inflammation and synaptic loss as the disease progresses. Using CD68 staining as a marker for microglia/macrophage activation in the brain, we observed significantly increased CD68 immunoreactivity in the amygdala of the early AD mouse brain that was not significantly reduced by EV treatment (Fig. 6a;  $P < 0.05$  for AD vs WT groups); however, no significant differences among experimental groups were observed for CD68 in the mPFC region of the brain at that same time



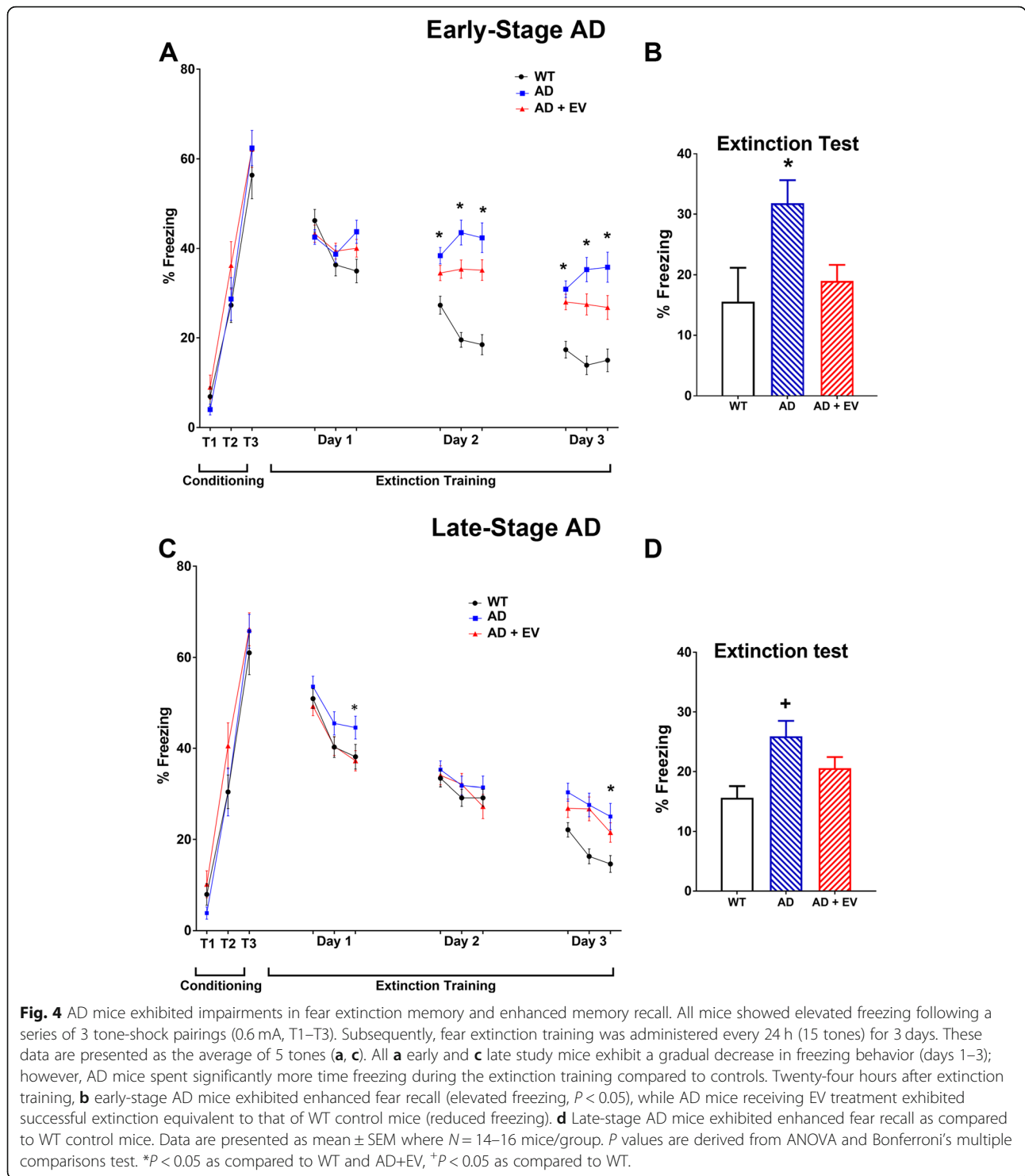


(Fig. 6b). As with the early AD mice, increased CD68 immunoreactivity was observed in the amygdala region of the brains of late AD mice, with only a trend for modulation by EV treatment (Fig. 6c, e–g;  $P < 0.01$  AD vs WT groups). Unlike the early AD

mice, though, late AD mice exhibit significant increases in CD68 immunoreactivity in the mPFC that were attenuated to control levels by EV treatment (Fig. 6d, h–j;  $P < 0.01$  for AD vs either WT or AD+EV groups).

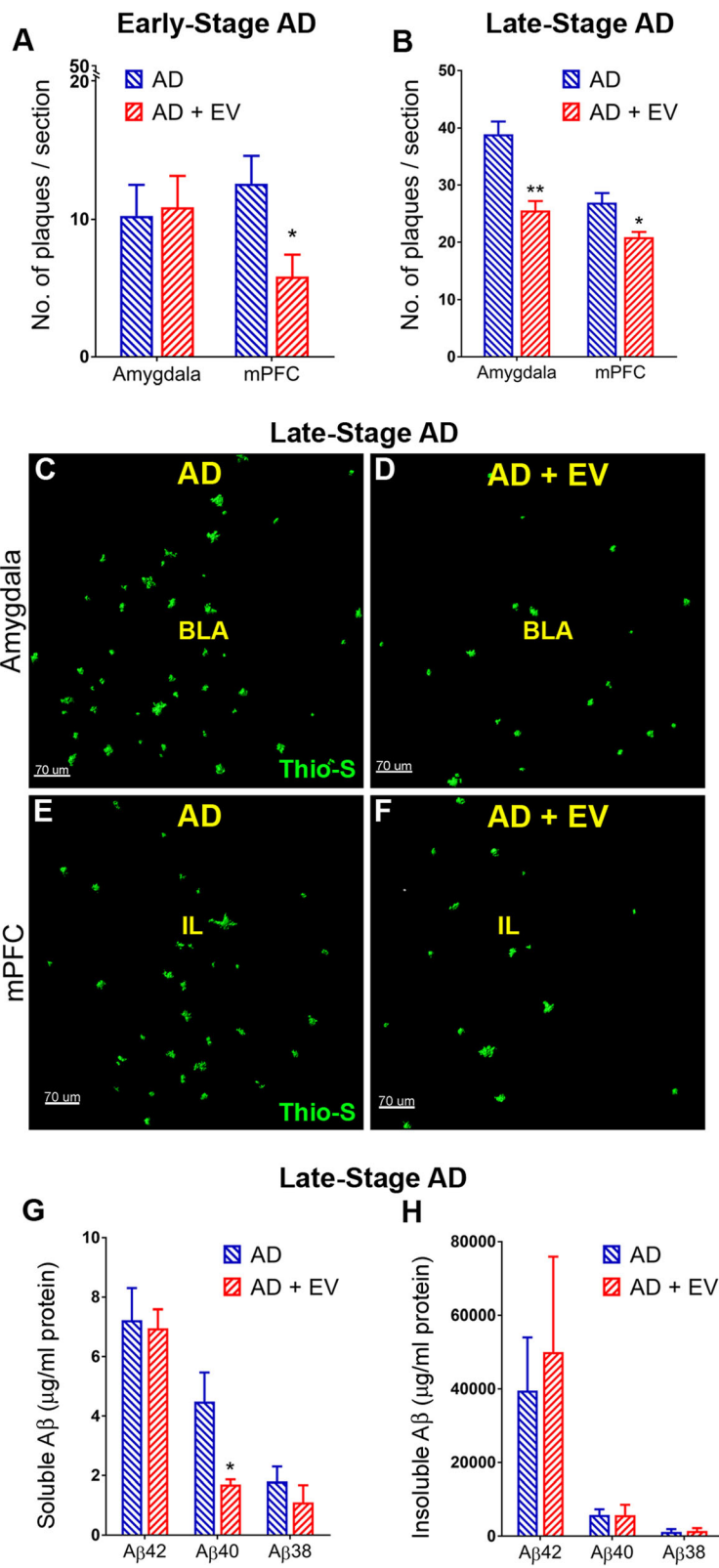


Fig. 5 (See legend on next page.)

(See figure on previous page.)

**Fig. 5** Dense core A $\beta$  plaque number was reduced in AD mice that received EV treatment. **a** Early-stage AD mice exhibited increased numbers of A $\beta$  plaques in the amygdala that were reduced by EV treatment and **b** late-stage AD mice exhibited increased numbers of A $\beta$  plaques in both the amygdala and the medial prefrontal cortex (mPFC) that were reduced by EV treatment. Representative images of Thio-S staining for late-stage AD and AD+EV mice qualitatively demonstrate late AD neuropathology as shown by the accumulation of A $\beta$  plaques in the **c** amygdala and **e** mPFC that were reduced in both the **d** amygdala and **f** mPFC regions of the AD brain by EV treatment (basal lateral amygdala, BLA; infralimbic cortex, IL; ABP, green). **g** A $\beta$  multiplex ELISA indicated the elevation of soluble A $\beta$ 40 in brain lysates that was significantly reduced by EV treatment, **h** while no changes were observed between AD and AD+EV mice in levels of insoluble A $\beta$ . Data are presented as mean  $\pm$  SEM (Thio-S,  $N = 4$  mice/group; ELISA,  $N = 7$  mice/group).  $P$  values derived from unpaired Student's  $t$  tests. \* $P < 0.05$ , \*\* $P < 0.01$  as compared to AD. Scale bar = 70  $\mu$ m

### EV treatment restored synaptophysin in the AD brain

Significant loss of pre- and post-synaptic proteins, such as pre-synaptic density protein-95 and synaptophysin, respectively, has been linked to the cognitive impairments associated with AD. Evaluation of synaptophysin immunoreactivity by confocal microscopy and volumetric quantification revealed significant decreases in this pre-synaptic marker in both the amygdala and the mPFC in the early AD brain that was restored to WT control levels in the EV-treated AD brain (Fig. 7a, b;  $P < 0.05$  for AD vs either WT or AD+EV groups). Similar, reductions were observed in the amygdala of the late AD brain that was also restored to WT levels by EV treatment (Fig. 7c, e–g;  $P < 0.05$  for AD vs either WT or AD+EV groups). While no significant differences in synaptophysin were observed in the comparison of the mPFC region of the brain for the WT and AD groups of late AD mice, the EV treatment increased the levels of synaptophysin to greater than that of either WT or AD mice (Fig. 7d, h–j;  $P < 0.05$  for AD vs AD+EV groups).

### The effect of EVs on peripheral inflammatory responses in AD

The increased neuroinflammation observed in AD is frequently associated with significant peripheral immune responses that correlate with adverse outcomes in human AD patients [3]. Therefore, the levels of inflammatory and anti-inflammatory cytokines in the plasma were evaluated. Interferon- $\gamma$  (IFN $\gamma$ ) is a pro-inflammatory cytokine that has been shown to prime microglia under pathological conditions including AD. While it remained unaffected in the early AD spleen, IFN $\gamma$  was upregulated in the late-stage AD spleen, and EV treatment significantly reduced those levels (Fig. 8a;  $P < 0.05$  for AD vs AD+EV groups). IL-17 overexpression has similarly been implicated in neuropathologies and AD. It was also found to be unaltered in early-stage AD, but significantly elevated in the late AD mice, and reduced WT levels by EV treatment (Fig. 8b;  $P < 0.05$  for AD vs AD+EV groups). Conversely, the anti-inflammatory cytokine IL-10 that downregulates the expression of inflammatory cytokines was found to be dramatically reduced in early-stage AD mice as compared to either WT or EV+AD mice (Fig. 8c;  $P < 0.01$  and  $P < 0.05$ , respectively for AD vs WT and AD+EV). It has been shown that the ratio of IgM

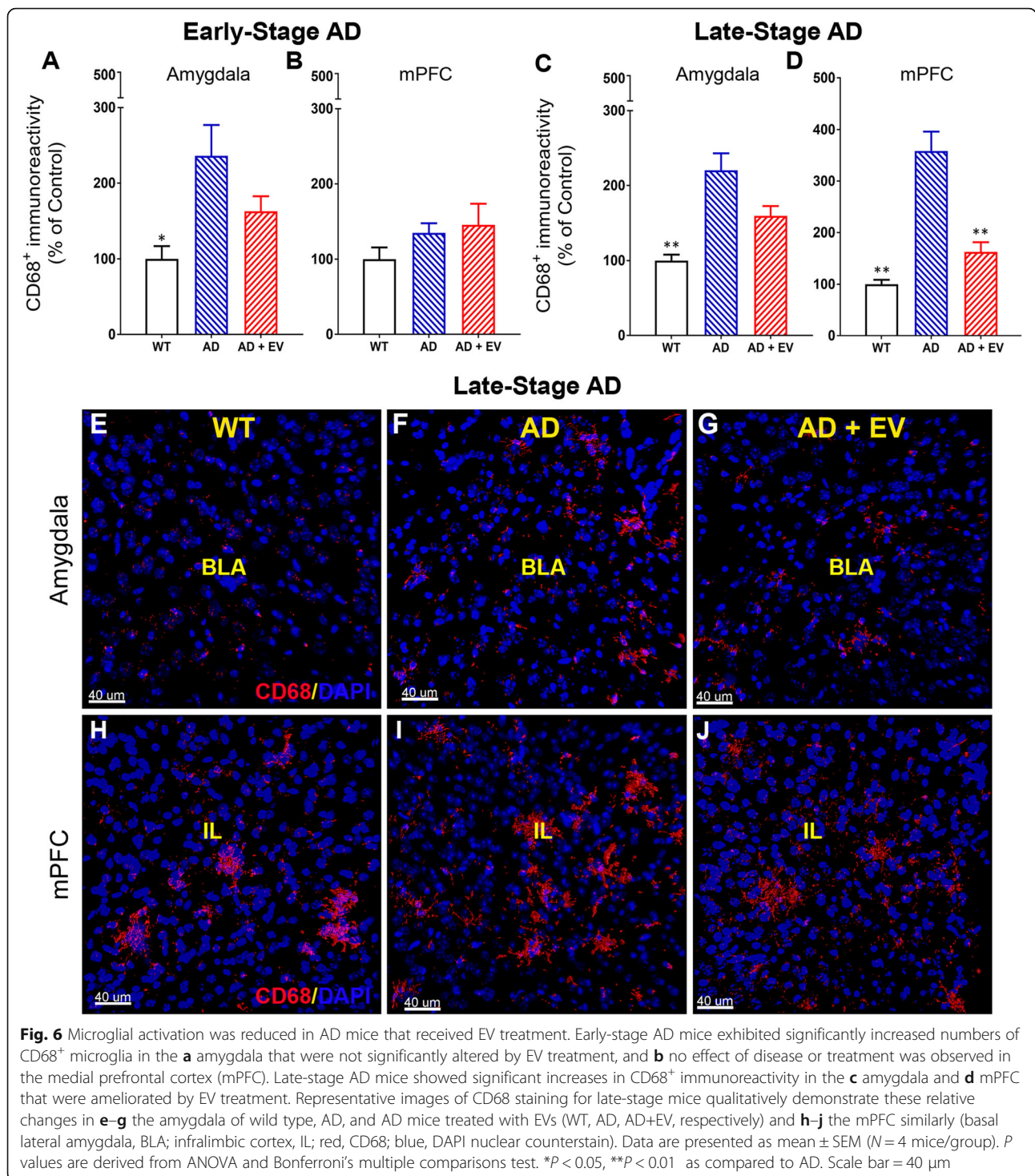
to IgG is significantly decreased in human AD patients and in the 5xFAD mouse model of AD [3]. A specialized subset of B1 cells produce IgM, the percentage of which was shown to be reduced in the AD mouse. Similarly, in this study, while not significant, a trend for decreased B1 cells was observed in late-stage AD mice as compared to WT or AD+EV mice (Fig. 8d).

### Effect of EV treatment on mRNA levels in the hippocampus of the AD brain

Significant changes in transcription levels of genes implicated in AD pathology have been observed previously. In the current study, increases in expression for genes involved in microglial activation (Fig. 9a), pro-inflammatory signaling (Fig. 9b), and immune responses (Fig. 9c) were noted when comparing WT and late-stage AD groups of mice. Statistical comparison of AD and AD+EV mice demonstrated a subtle trend for the effectiveness of the EV treatment in certain animals; however, one AD+EV mouse remained a consistent non-responder to EV treatment, exhibiting high levels of expression for all AD-related genes evaluated.

### miRNA microarray analysis reveals potential therapeutic EV cargo

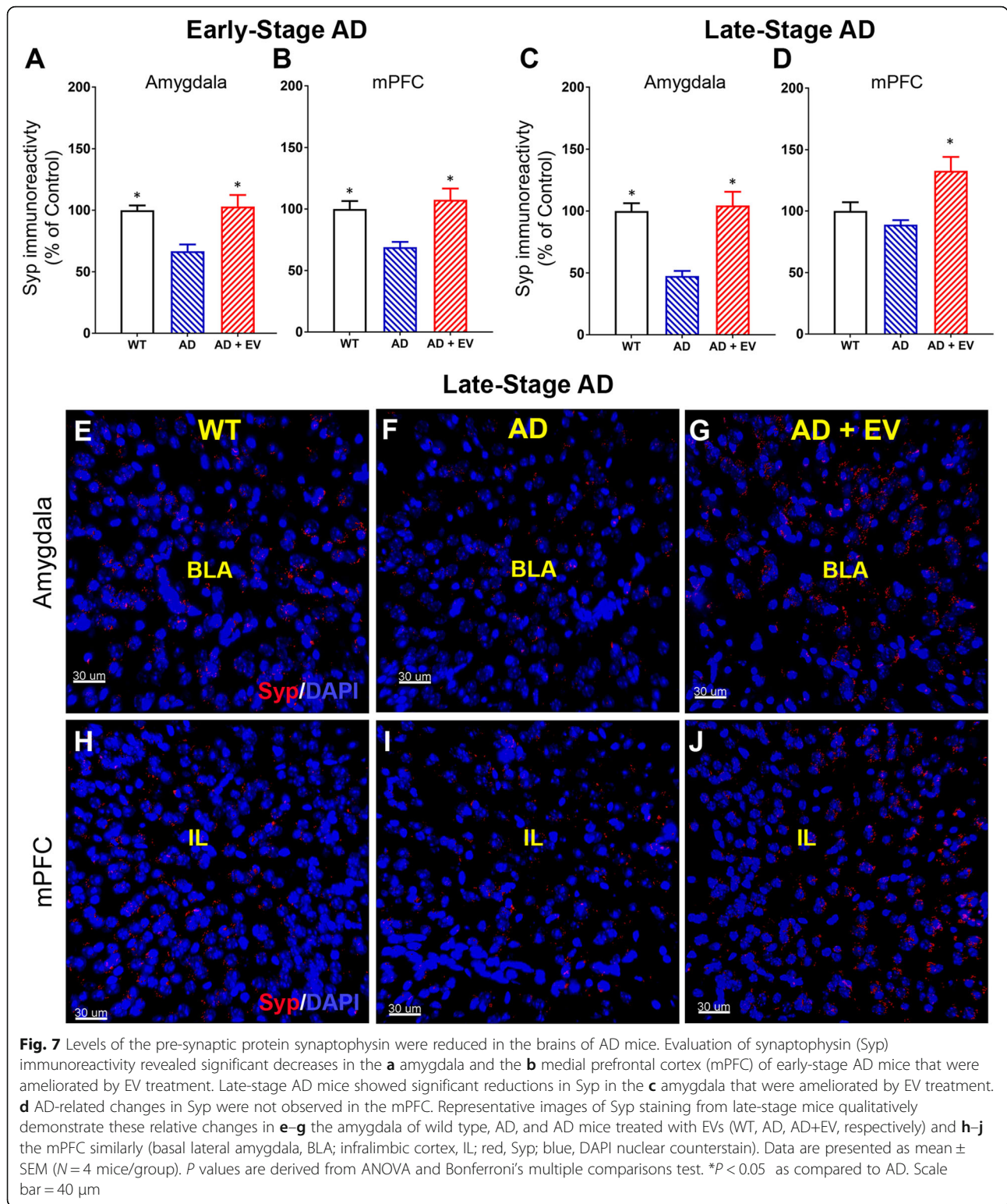
To investigate potential functional components of hNSC-derived EVs, miRNA cargo was evaluated using a targeted human miRNA array [11] (Supplemental Table 2). Candidate miRNA implicated in AD-related pathways including learning, memory, and neuroinflammation were identified by cross-referencing the array data with the literature, which vary widely in opinions regarding the pathways influenced by a particular miRNA and whether the effect is beneficial or detrimental to CNS homeostasis or pathology. Among the miRNA identified in this analysis were miR-125b-5p, miR-124-3p, and miR-125a-5p (Table 1). All of these select candidates were confirmed to be present in EV RNA samples using TaqMan Advanced miRNA Assays, providing candidate miRNA for potential follow-up studies that could influence CNS function [55–57].



### Discussion

AD is an irreversible neurodegenerative disease for which there are currently no effective therapies to slow or reverse the disease progression. A typical hallmark of AD is the accumulation of Aβ plaques that leads to persistent microglial activation creating a pro-inflammatory, neurotoxic environment that ultimately causes cognitive and

functional decline and memory loss. Our past work has defined the effects of clinically relevant radiation exposures on the brain, which include cognitive impairment, neuroinflammation, dysregulation of pre- or post-synaptic protein levels, and loss of neuronal structure [5, 6]. Work then demonstrated that cranially grafted hNSC and then hNSC-derived EVs were effective in mitigating radiation-



induced neurodegenerative events. Here, we have demonstrated that the same hNSC-derived EV therapy is effective in ameliorating AD-related neurodegenerative pathologies. Single or duplicate EV treatments were found

to reverse cognitive impairments in AD mice, including anxiety-like behaviors and fear memory consolidation. One of the hallmarks of AD pathology is a progressive accumulation of A $\beta$  plaques in the brain. While plaque

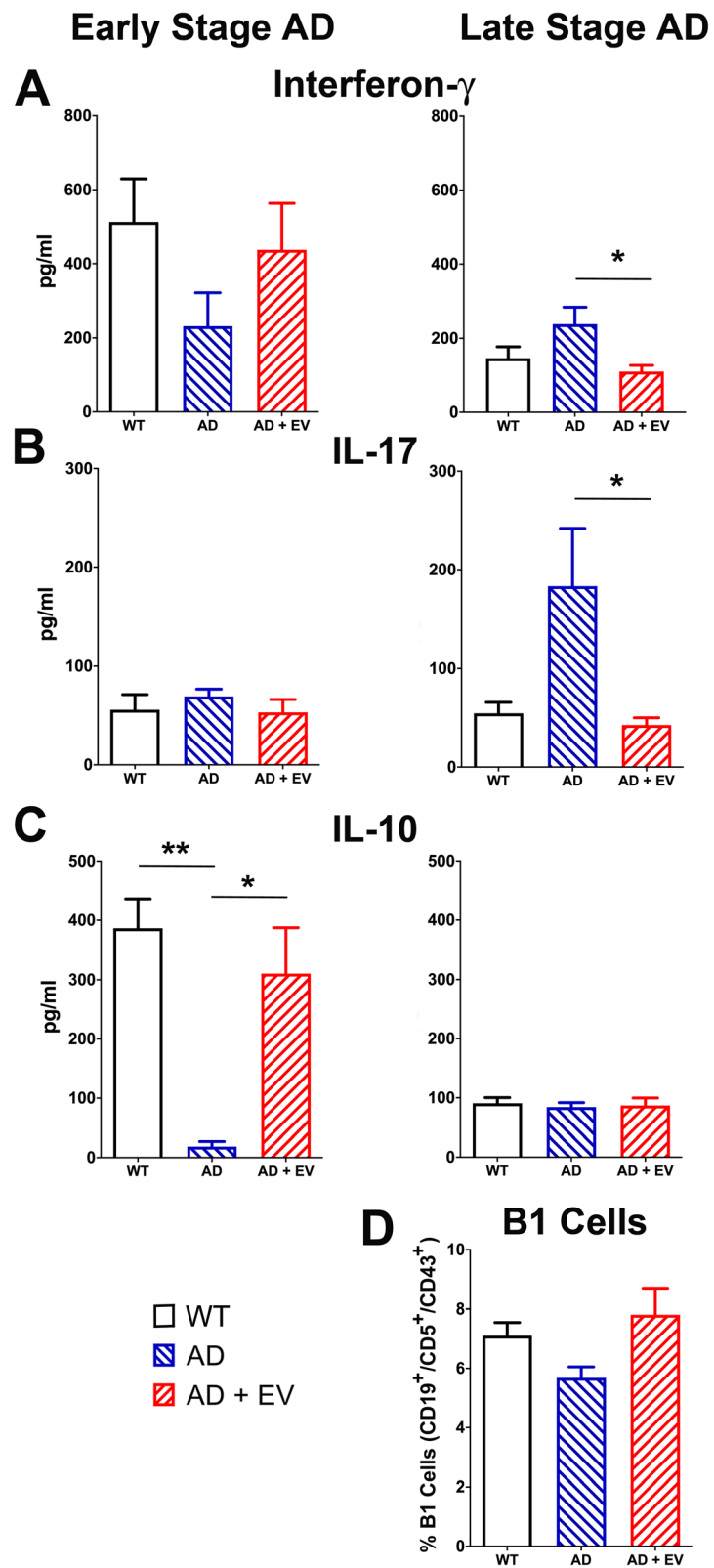


Fig. 8 (See legend on next page.)

(See figure on previous page.)

**Fig. 8** Elevated levels of inflammatory cytokines in AD mice were reduced by EV treatment. Levels of cytokines secreted by PMA- and ionomycin-stimulated spleen cells were measured in WT, AD, and AD+EV mice. **a, b** While unaffected in early-stage AD mice, interferon- $\gamma$  and IL-17 pro-inflammatory cytokines were significantly elevated in late-stage AD mice and significantly reduced by EV treatment. **c** Alternatively, reduced levels of the anti-inflammatory cytokine IL-10 in early-stage AD mice were restored to nearly control levels in the AD mice that received EV treatment. No changes among groups were observed for IL-10 in the late-stage animals. **d** Spleen cells were also stained for B1 cells (CD19<sup>+</sup>, CD5<sup>+</sup>, CD43<sup>+</sup>) and analyzed by flow cytometry. While not statistically significant, a trend for a reduced percentage of B1 cells was observed for AD mice and improved by EV treatment. Data are presented as mean  $\pm$  SEM ( $N = 7$  mice/group).  $P$  values are derived from ANOVA and Bonferroni's multiple comparisons test. \* $P < 0.05$ , \*\* $P < 0.01$

density is not directly linked with dementia [58, 59], the neurodegenerative effects of plaques in triggering neuroinflammation and loss of neurons are well documented [4, 60, 61]. To delineate the regenerative effects of stem cell-derived EVs on pathology, whole-brain ELISA on late-stage AD brains was employed and revealed significant reductions in the levels of soluble amyloid- $\beta_{1-40}$ , that along with  $A\beta_{1-42}$ , is a robust predictor of AD-related synaptic loss [62–64]. While it is unclear why no changes in levels of  $A\beta_{1-42}$ , our Thio-S staining for dense core  $A\beta$  plaques confirmed that EV treatment provided some reductions in plaque load. These data indicate that the neuroprotective effects of EVs are exerted, in part, by reducing the plaque burden in the AD brain at early and late stages of disease progression.

Persistent activation of microglia in the AD brain is detrimental to neuronal and cognitive function. Our past data have shown anti-inflammatory effects of stem cells or stem cell-derived EVs in clinically relevant irradiation [8, 9, 65] and chemobrain [66] models. Substantiating the neuroprotective impact of EVs in the AD brain, we found significant reductions in the levels of CD68, a marker of microglial/myeloid cell activation. While we did not evaluate neuron structure in the current study, persistent microglial reactivity has been linked to synapse loss in AD [61, 67, 68]. Mouse models of AD, including the 5xFAD model, have also been found to have reduced levels of pre- and post-synaptic protein levels. Our data demonstrated significant reductions in synaptophysin immunoreactivity in the AD brain that were restored by EV treatment. Together, these data in an AD model, as well as our studies of EV amelioration of radiation-induced brain injury, suggest dysfunction of neural circuitry in the hippocampus, mPFC, and amygdala that could be ameliorated by EV treatment [10–12].

Inflammatory markers from the peripheral immune response indicate a highly pro-inflammatory environment in AD mice that could be mitigated in part by EV treatment. IFN $\gamma$  and IL-17 are highly inflammatory cytokines, and both implicated in CNS-related disorders such as multiple sclerosis. Reduction in IL-17 is especially important as IL-17 has been shown to cause neuronal cell death in the human Parkinson's disease iPSC model [69]. Decreased levels of IL-10 levels, an anti-

inflammatory cytokine in early AD, also indicate an impairment in controlling inflammation. Reductions in B1 cells in late-stage AD may also contribute to AD-related accumulation of  $A\beta$  plaques as these cells contribute significantly to the removal of cell debris and self-proteins. Restoration of B1 cell frequencies and reduced IFN $\gamma$  and IL-17 by EVs at late-stage AD combined with increased IL-10 levels at the early stage indicates that EV treatment is affecting multiple pathways to dampen inflammation.

The cognitive and molecular observations from this study are supported by gene expression analysis from the late-stage AD brain that demonstrated consistent increases in mRNA levels for genes involved in microglial activation, inflammation, and other AD pathologies. Critically, the two EV treatments to the late-stage AD mouse resulted in strong trends for reductions in that gene overexpression as compared to AD only mice.

An important part of this study is the analysis and identification of potentially beneficial EV cargo. Array analysis identified at least 3 strong candidate miRNA, miR-125a, miR-125b, and miR-124. While overexpression of any of these candidate miRNA can be damaging in specific cases [47], literature has also suggested they serve beneficial roles in the CNS. MiR-125a and miR-125b have been shown to maintain PSD-95 levels in dendrites and regulate synaptic structure, and miR-125b is an important regulator of synaptic structure and function [52, 54]. MiR-124 was the clear lead candidate EV miRNA in the context of ameliorating the hallmarks of AD. MiR-124 expression has been demonstrated to reduce neuroinflammation and promote neurite outgrowth in traumatic brain injury models [20, 48–50]. Further, miR-124 has been suggested to regulate glycogen synthase kinase 3 $\beta$  and glucocorticoid receptor levels in the context of AD (GSK3 $\beta$  and GR, respectively) and regulate anxiety as well as impulse control disorders that are indicative of poor decision-making in humans [51]. The reported downregulation of miR-124 in the AD brain may, at least in part, contribute to the neuropathological phenotypes associated with AD. Significantly, we have recently demonstrated that AAV9-mediated overexpression of miR-124 alone was able to reduce the neurodegenerative consequences of cranial irradiation on

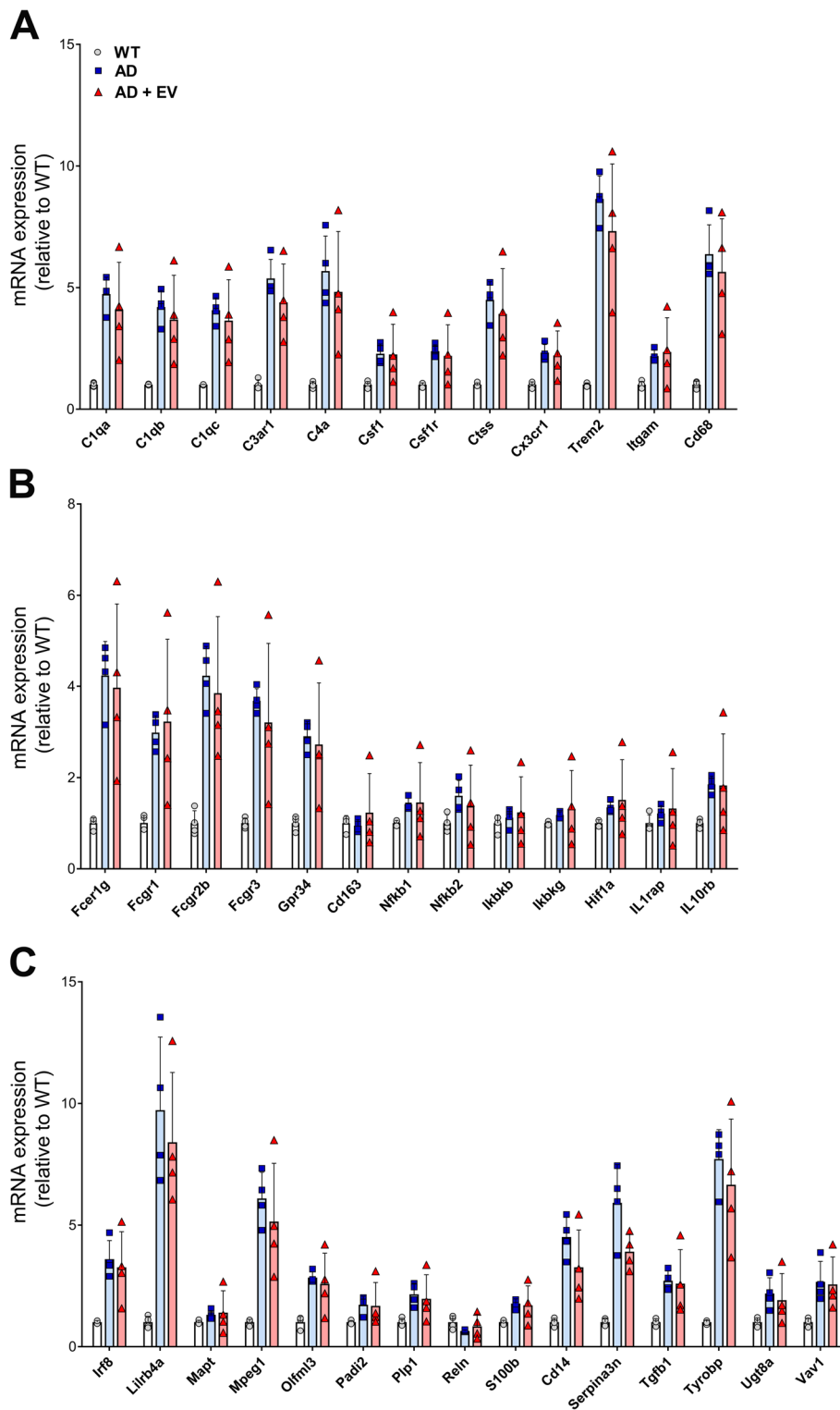


**Fig. 9** Gene expression in the hippocampus of late-stage AD mice. Analysis of **a** microglial, **b** pro-inflammation, **c** immune response, and other mRNA levels demonstrated increased gene expression in the hippocampus of late-stage AD mice as compared to WT controls. Those elevated mRNA levels were reduced in some, but not all AD+EV-treated mice. Data are presented as mean  $\pm$  SEM ( $N = 4$  mice/group)



**Table 1** Candidate microRNA EV cargo

MicroRNA	Average miR expression (log scale)	Relevance to AD	Reference
MiR-124-3p	20,761.5	<b>Inhibition of neural inflammation in the damaged brain Downregulated in AD and neurodegenerative diseases</b>	[20, 47–51]
MiR-125b-5p	22,278.9	Normal expression attenuates A $\beta$ -induced toxicity, reduces apoptosis and oxidative stress Regulates PSD-95 levels	[52, 53]
MiR-125a-5p	5284.8	Downregulation decreases levels of PSD-95 in dendrites and dendrite complexity	[54]
Neg control 1	726.0		
Neg control 2	709.0		
Neg control 3	688.5		

cognition and microglial activation [11]. We hypothesize that similar pathways may be at play in the AD brain, where miR-124 helps to resolve a wide range of neuropathologies.

Similar observations regarding the efficacy of EVs in the treatment of AD have been made by other laboratories as well. Li and colleagues used embryonic mouse NSC-derived EVs to treat 9-month-old B6C3-tg mice via stereotactic injection into the lateral ventricles [14]. Five weeks later, AD mice treated with EVs were shown to have improved performance on the Morris water maze as compared to untreated AD littermates. Similarly, the EV treatment increased the levels of synaptic proteins, including synaptophysin and PSD-95, and improved synaptic morphology and mitochondrial function. While the EV treatment also reduced the levels of pro-inflammatory cytokines, it did not reduce the A $\beta$  plaque load, supporting the assertion that plaques might not drive the cognitive phenotype of AD. Using mouse mesenchymal stem cell-derived EVs, Losurdo and colleagues administered two intranasal doses to 3xTg AD mice and found a shift towards an anti-inflammatory phenotype and reduced activation of microglia, as well as improved dendritic spine density [15]. These examples using two distinct models of AD corroborate our data on the beneficial effects of systemic injections of EVs on disease pathology.

### Limitations

While we do not see complete remediation of cognitive function, one or two injections of EVs were able to partially restore cognitive indices in male 5xFAD mice. Our current observations suggest that additional, ongoing treatments with the EVs could improve the efficacy of the therapy, forestalling or even reversing AD pathologies. Additional studies are needed to confirm the efficacy of this same EV therapeutic strategy in the treatment AD in female mice. Importantly, we emphasize that our studies provide indications of at least one of the mechanisms by which these hNSC-derived EVs may repair the AD

brain, delivering miRNA capable of reducing inflammation and protecting neuronal structure, possibly through epigenetic regulation of gene expression. We acknowledge that other cargo is likely to play a role in the effectiveness of these EVs and future studies will focus not only on the miRNA cargo and mechanisms but also on the other potentially beneficial EV cargo such as protein.

### Conclusion

AD is an irreversible neurodegenerative disease affecting millions of people worldwide, and regenerative therapies to mitigate AD neuropathology have shown very limited success. The findings of this study demonstrate the neuroprotective efficacy of systemic administration of stem cell-derived EVs for remediation of behavioral and molecular AD neuropathologies. Further, these data suggest that EV-contained miRNA may represent a potential, specific mechanism for follow-up studies to develop therapeutic strategies to meet this critical unmet medical need.

### Supplementary Information

The online version contains supplementary material available at <https://doi.org/10.1186/s13195-021-00791-x>.

#### Additional file 1.

### Abbreviations

A $\beta$ : Amyloid-beta; AD: Alzheimer's disease; BLA: Basal lateral amygdala; CNS: Central nervous system; ELISA: Enzyme-linked immunosorbent assay; EPM: Elevated plus maze; EV: Extracellular vesicle; FE: Fear extinction; HSCRO: Human Stem Cell Research Oversight Committee; hNSC: Human neural stem cell; IL: Infralimbic cortex; IFN $\gamma$ : Interferon gamma; IL: Interleukin; LDB: Light-dark box; MiR, miRNA: MicroRNA; mPFC: Medial prefrontal cortex; NIH: National Institute of Health; NOR: Novel object recognition; PFA: Paraformaldehyde; PSD-95: Post-synaptic density protein-95; RO: Retro-orbital; Syp: Synaptophysin; Thio-S: Thioflavin-s; WT: Wild type

### Acknowledgements

We acknowledge contributions from Drs. Matthew Blurton-Jones and Hayk Davtyan including guidance and stimulating discussions regarding this project and for technical assistance. We also acknowledge Dr. Ron Leavitt for the miRNA data analysis and validation and Drs. William Janssen and Dara Dickstein for electron microscopy analysis of EV.

**Authors' contributions**

Conception and design: JEB and MMA. Development of methodology: AA. Acquisition of data: LAA, AADB, CG, LA, EG, and NR. Analysis and interpretation of data: LAA, AADB, AA, MMA, and JEB. Writing, review, and/or revision of the manuscript: AA, JEB, and MMA. Administrative, technical, or material support: EG, NR, and MMA. Study supervision: JEB and MMA. The authors read and approved the final manuscript.

**Funding**

This work was supported by the UCI Research Seed Funding Program and the California Institute for Regenerative Medicine (DISC1-10079) to JEB.

**Availability of data and materials**

Correspondence and request for data or materials should be addressed to JEB.

**Ethics approval and consent to participate**

Not applicable

**Consent for publication**

Not applicable

**Competing interests**

The authors declare no competing interests.

**Author details**

<sup>1</sup>Department of Radiation Oncology, University of California Irvine, Irvine, CA 92697, USA. <sup>2</sup>Department of Medicine, University of California Irvine, Irvine, CA 92697, USA.

Received: 19 November 2020 Accepted: 16 February 2021

Published online: 06 March 2021

**References**

- LaFerla FM, Green KN. Animal models of Alzheimer disease. *Cold Spring Harb Perspect Med.* 2012;2(11):a006320. <https://doi.org/10.1101/cshperspect.a006320>.
- Alam Q, Alam MZ, Mushtaq G, Damanhoury GA, Rasool M, Kamal MA, Haque A. Inflammatory process in Alzheimer's and Parkinson's diseases: central role of cytokines. *Curr Pharm Des.* 2016;22:541–8.
- Baulch JE, Acharya MM, Agrawal S, Apodaca LA, Monteiro C, Agrawal A. Immune and inflammatory determinants underlying Alzheimer's disease pathology. *J NeuroImmune Pharmacol.* 2020;15(4):852–62. <https://doi.org/10.1007/s11481-020-09908-9>.
- Spangenberg EE, Lee RJ, Najafi AR, Rice RA, Elmore MR, Blurton-Jones M, West BL, Green KN. Eliminating microglia in Alzheimer's mice prevents neuronal loss without modulating amyloid-beta pathology. *Brain.* 2016;139:1265–81.
- Parihar VK, Pasha J, Tran KK, Craver BM, Acharya MM, Limoli CL. Persistent changes in neuronal structure and synaptic plasticity caused by proton irradiation. *Brain Struct Funct.* 2014;220(2):1161–71. <https://doi.org/10.1007/s00429-014-0709-9>.
- Acharya MM, Roa DE, Bosch O, Lan ML, Limoli CL. Stem cell transplantation strategies for the restoration of cognitive dysfunction caused by cranial radiotherapy. *J Vis Exp.* 2011;(56):3107. <https://doi.org/10.3791/3107>.
- Acharya MM, Christie LA, Lan ML, Limoli CL. Comparing the functional consequences of human stem cell transplantation in the irradiated rat brain. *Cell Transplant.* 2013;22:55–64.
- Acharya MM, Rosi S, Jopson T, Limoli CL. Human neural stem cell transplantation provides long-term restoration of neuronal plasticity in the irradiated hippocampus. *Cell Transplant.* 2014;24(4):691–702. <https://doi.org/10.3727/096368914X684600>.
- Acharya MM, Martirosian V, Christie LA, Riparip L, Strnadel J, Parihar VK, Limoli CL. Defining the optimal window for cranial transplantation of human induced pluripotent stem cell-derived cells to ameliorate radiation-induced cognitive impairment. *Stem Cells Transl Med.* 2015;4:74–83.
- Baulch JE, Acharya MM, Allen BD, Ru N, Chmielewski NN, Martirosian V, Giedzinski E, Syage A, Park AL, Benke SN, et al. Cranial grafting of stem cell-derived microvesicles improves cognition and reduces neuropathology in the irradiated brain. *Proc Natl Acad Sci U S A.* 2016;113:4836–41.
- Leavitt RJ, Acharya MM, Baulch JE, Limoli CL. Extracellular vesicle-derived miR-124 resolves radiation-induced brain injury. *Cancer Res.* 2020;80(19):4266–77. <https://doi.org/10.1158/0008-5472.CAN-20-1599>.
- Smith SM, Giedzinski E, Angulo MC, Lui T, Lu C, Park AL, Tang S, Martirosian V, Ru N, Chmielewski NN, et al. Functional equivalence of stem cell and stem cell-derived extracellular vesicle transplantation to repair the irradiated brain. *Stem Cells Transl Med.* 2020;9:93–105.
- Marsh SE, Blurton-Jones M. Neural stem cell therapy for neurodegenerative disorders: the role of neurotrophic support. *Neurochem Int.* 2017;106:94–100.
- Li B, Liu J, Gu G, Han X, Zhang Q, Zhang W. Impact of neural stem cell-derived extracellular vesicles on mitochondrial dysfunction, sirtuin 1 level, and synaptic deficits in Alzheimer's disease. *J Neurochem.* 2020;154:502–18.
- Losurdo M, Pedrazzoli M, D'Agostino C, Elia CA, Massenzio F, Lonati E, Mauri M, Rizzi L, Molteni L, Bresciani E, Dander E, D'Amico G, Bulbarelli A, Torsello A, Matteoli M, Buffelli M, Coco S. Intranasal delivery of mesenchymal stem cell-derived extracellular vesicles exerts immunomodulatory and neuroprotective effects in a 3xTg model of Alzheimer's disease. *Stem Cells Transl Med.* 2020;9(9):1068–84. <https://doi.org/10.1002/sctm.19-0327>.
- Colombo M, Raposo G, Thery C. Biogenesis, secretion, and intercellular interactions of exosomes and other extracellular vesicles. *Annu Rev Cell Dev Biol.* 2014;30:255–89.
- Andaloussi S, Mager I, Breakefield XO, Wood MJ. Extracellular vesicles: biology and emerging therapeutic opportunities. *Nat Rev Drug Discov.* 2013;12:347–57.
- Prada I, Gabrielli M, Turola E, Iorio A, D'Arrigo G, Parolisi R, De Luca M, Pacifici M, Bastoni M, Lombardi M, et al. Glia-to-neuron transfer of miRNAs via extracellular vesicles: a new mechanism underlying inflammation-induced synaptic alterations. *Acta Neuropathol.* 2018;135:529–50.
- Soares Martins T, Trindade D, Vaz M, Campelo I, Almeida M, Trigo G, da Cruz ESOAB, Henriques AG. Diagnostic and therapeutic potential of exosomes in Alzheimer's disease. *J Neurochem.* 2020;156(2):162–81. <https://doi.org/10.1111/jnc.15112>.
- Li D, Huang S, Yin Z, Zhu J, Ge X, Han Z, Tan J, Zhang S, Zhao J, Chen F, et al. Increases in miR-124-3p in microglial exosomes confer neuroprotective effects by targeting FIP200-mediated neuronal autophagy following traumatic brain injury. *Neurochem Res.* 2019;44:1903–23.
- Zhang G, Zhu Z, Wang H, Yu Y, Chen W, Waqas A, Wang Y, Chen L. Exosomes derived from human neural stem cells stimulated by interferon gamma improve therapeutic ability in ischemic stroke model. *J Adv Res.* 2020;24:435–45.
- Zhang W, Egashira N, Masuda S. Recent topics on the mechanisms of immunosuppressive therapy-related neurotoxicities. *Int J Mol Sci.* 2019;20(13):3210.
- Blum B, Benvenisty N. The tumorigenicity of human embryonic stem cells. *Adv Cancer Res.* 2008;100:133–58.
- Bradley JA, Bolton EM, Pedersen RA. Stem cell medicine encounters the immune system. *Nat Rev Immunol.* 2002;2:859–71.
- Gutierrez-Aranda I, Ramos-Mejia V, Bueno C, Munoz-Lopez M, Real PJ, Macia A, Sanchez L, Ligerio G, Garcia-Perez JL, Menendez P. Human induced pluripotent stem cells develop teratoma more efficiently and faster than human embryonic stem cells regardless the site of injection. *Stem Cells.* 2010;28:1568–70.
- Mollison KW, Fey TA, Krause RA, Andrews JM, Bretheim PT, Cusick PK, Hsieh GC, Luly JR. Nephrotoxicity studies of the immunosuppressants tacrolimus (FK506) and ascomycin in rat models. *Toxicology.* 1998;125:169–81.
- Oakley H, Cole SL, Logan S, Maus E, Shao P, Craft J, Guillozet-Bongaarts A, Ohno M, Disterhoft J, Van Eldik L, et al. Intraneuronal beta-amyloid aggregates, neurodegeneration, and neuron loss in transgenic mice with five familial Alzheimer's disease mutations: potential factors in amyloid plaque formation. *J Neurosci.* 2006;26:10129–40.
- Acharya MM, Lan ML, Kan VH, Patel NH, Giedzinski E, Tseng BP, Limoli CL. Consequences of ionizing radiation-induced damage in human neural stem cells. *Free Radic Biol Med.* 2010;49:1846–55.
- Thery C, Amigorena S, Raposo G, Clayton A. Isolation and characterization of exosomes from cell culture supernatants and biological fluids. *Curr Protoc Cell Biol* 2006, Chapter 3:Unit 3.22.
- Long Q, Upadhyay D, Hattiangady B, Kim DK, An SY, Shuai B, Prockop DJ, Shetty AK. Intranasal MSC-derived A1-exosomes ease inflammation, and prevent abnormal neurogenesis and memory dysfunction after status epilepticus. *Proc Natl Acad Sci U S A.* 2017;114:E3536–45.

31. Xin H, Li Y, Cui Y, Yang JJ, Zhang ZG, Chopp M. Systemic administration of exosomes released from mesenchymal stromal cells promote functional recovery and neurovascular plasticity after stroke in rats. *J Cereb Blood Flow Metab.* 2013;33:1711–5.
32. Yang J, Zhang X, Chen X, Wang L, Yang G. Exosome mediated delivery of miR-124 promotes neurogenesis after ischemia. *Mol Ther Nucleic Acids.* 2017;7:278–87.
33. Zhang Y, Chopp M, Zhang ZG, Katakowski M, Xin H, Qu C, Ali M, Mahmood A, Xiong Y. Systemic administration of cell-free exosomes generated by human bone marrow derived mesenchymal stem cells cultured under 2D and 3D conditions improves functional recovery in rats after traumatic brain injury. *Neurochem Int.* 2016;111:69–81. <https://doi.org/10.1016/j.neuint.2016.08.003>.
34. Acharya MM, Christie LA, Lan ML, Donovan PJ, Cotman CW, Fike JR, Limoli CL. Rescue of radiation-induced cognitive impairment through cranial transplantation of human embryonic stem cells. *Proc Natl Acad Sci U S A.* 2009;106:19150–5.
35. Kalani A, Chaturvedi P, Kamat PK, Maldonado C, Bauer P, Joshua IG, Tyagi SC, Tyagi N. Curcumin-loaded embryonic stem cell exosomes restored neurovascular unit following ischemia-reperfusion injury. *Int J Biochem Cell Biol.* 2016;79:360–9.
36. Drommelschmidt K, Serdar M, Bendix I, Herz J, Bertling F, Prager S, Keller M, Ludwig AK, Duhan V, Radtke S, et al. Mesenchymal stem cell-derived extracellular vesicles ameliorate inflammation-induced preterm brain injury. *Brain Behav Immun.* 2017;60:220–32.
37. Barker GR, Warburton EC. When is the hippocampus involved in recognition memory? *J Neurosci.* 2011;31:10721–31.
38. Barker GR, Bird F, Alexander V, Warburton EC. Recognition memory for objects, place, and temporal order: a disconnection analysis of the role of the medial prefrontal cortex and perirhinal cortex. *J Neurosci.* 2007;27:2948–57.
39. Bourin M, Hascoet M. The mouse light/dark box test. *Eur J Pharmacol.* 2003;463:55–65.
40. Bourin M. Animal models for screening anxiolytic-like drugs: a perspective. *Dialogues Clin Neurosci.* 2015;17:295–303.
41. Walf AA, Frye CA. The use of the elevated plus maze as an assay of anxiety-related behavior in rodents. *Nat Protoc.* 2007;2:322–8.
42. Acharya MM, Baulch JE, Klein PM, Baddour AAD, Apodaca LA, Kramár EA, Alikhani L, Garcia C Jr, Angulo MC, Batra RS, Fallgren CM, Borak TB, Stark CEL, Wood MA, Britten RA, Soltesz I, Limoli CL. New Concerns for Neurocognitive Function during Deep Space Exposures to Chronic, Low Dose-Rate, Neutron Radiation. *eNeuro.* 2019;6(4):ENEURO.0094-19.2019. <https://doi.org/10.1523/ENEURO.0094-19.2019>.
43. Milad MR, Quirk GJ. Neurons in medial prefrontal cortex signal memory for fear extinction. *Nature.* 2002;420:70–4.
44. Khalsa DS. Stress, meditation, and Alzheimer's disease prevention: where the evidence stands. *J Alzheimers Dis.* 2015;48:1–12.
45. Bonardi C, de Pulford F, Jennings D, Pardon MC. A detailed analysis of the early context extinction deficits seen in APP<sup>swe</sup>/PS1<sup>dE9</sup> female mice and their relevance to preclinical Alzheimer's disease. *Behav Brain Res.* 2011;222:89–97.
46. Cain CK, Blouin AM, Barad M. Temporally massed CS presentations generate more fear extinction than spaced presentations. *J Exp Psychol Anim Behav Process.* 2003;29:323–33.
47. Sun Y, Luo ZM, Guo XM, Su DF, Liu X. An updated role of microRNA-124 in central nervous system disorders: a review. *Front Cell Neurosci.* 2015;9:193.
48. Huang S, Ge X, Yu J, Han Z, Yin Z, Li Y, Chen F, Wang H, Zhang J, Lei P. Increased miR-124-3p in microglial exosomes following traumatic brain injury inhibits neuronal inflammation and contributes to neurite outgrowth via their transfer into neurons. *FASEB J.* 2018;32:512–28.
49. Yang Y, Ye Y, Kong C, Su X, Zhang X, Bai W, He X. MiR-124 enriched exosomes promoted the M2 polarization of microglia and enhanced Hippocampus neurogenesis after traumatic brain injury by inhibiting TLR4 pathway. *Neurochem Res.* 2019;44:811–28.
50. Yu A, Zhang T, Duan H, Pan Y, Zhang X, Yang G, Wang J, Deng Y, Yang Z. MiR-124 contributes to M2 polarization of microglia and confers brain inflammatory protection via the C/EBP- $\alpha$  pathway in intracerebral hemorrhage. *Immunol Lett.* 2017;182:1–11.
51. ArunSundar M, Shanmugarajan TS, Ravichandiran V. 3,4-Dihydroxyphenylethanol assuages cognitive impulsivity in Alzheimer's disease by attuning HPA-axis via differential crosstalk of alpha7 nAChR with microRNA-124 and HDAC6. *ACS Chem Neurosci.* 2018;9:2904–16.
52. Edbauer D, Neilson JR, Foster KA, Wang CF, Seeburg DP, Batterton MN, Tada T, Dolan BM, Sharp PA, Sheng M. Regulation of synaptic structure and function by FMRP-associated microRNAs miR-125b and miR-132. *Neuron.* 2010;65:373–84.
53. Li P, Xu Y, Wang B, Huang J, Li Q. miR-34a-5p and miR-125b-5p attenuate Abeta-induced neurotoxicity through targeting BACE1. *J Neurol Sci.* 2020;413:116793.
54. Muddashetty RS, Nalavadi VC, Gross C, Yao X, Xing L, Laur O, Warren ST, Bassell GJ. Reversible inhibition of PSD-95 mRNA translation by miR-125a, FMRP phosphorylation, and mGluR signaling. *Mol Cell.* 2011;42:673–88.
55. Lukiw WJ, Andreeva TV, Grigorenko AP, Rogavov EI. Studying micro RNA function and dysfunction in Alzheimer's disease. *Front Genet.* 2012;3:327.
56. Swarbrick S, Wragg N, Ghosh S, Stolzing A. Systematic review of miRNA as biomarkers in Alzheimer's disease. *Mol Neurobiol.* 2019;56:6156–67.
57. Tan L, Yu JT, Liu QY, Tan MS, Zhang W, Hu N, Wang YL, Sun L, Jiang T, Tan L. Circulating miR-125b as a biomarker of Alzheimer's disease. *J Neurol Sci.* 2014;336:52–6.
58. Nelson PT, Alafuzoff I, Bigio EH, Bouras C, Braak H, Cairns NJ, Castellani RJ, Crain BJ, Davies P, Del Tredici K, et al. Correlation of Alzheimer disease neuropathologic changes with cognitive status: a review of the literature. *J Neuropathol Exp Neurol.* 2012;71:362–81.
59. Serrano-Pozo A, Frosch MP, Masliah E, Hyman BT. Neuropathological alterations in Alzheimer disease. *Cold Spring Harb Perspect Med.* 2011;1:a006189.
60. Paolicelli RC, Bolasco G, Pagani F, Maggi L, Scianni M, Panzanelli P, Giustetto M, Ferreira TA, Guiducci E, Dumas L, et al. Synaptic pruning by microglia is necessary for normal brain development. *Science.* 2011;333:1456–8.
61. Spangenberg EE, Green KN. Inflammation in Alzheimer's disease: lessons learned from microglia-depletion models. *Brain Behav Immun.* 2017;61:1–11.
62. Lue LF, Beach TG, Walker DG. Alzheimer's disease research using human microglia. *Cells.* 2019;8(8):838. <https://doi.org/10.3390/cells8080838>.
63. Counts SE, Ikonomic MD, Mercado N, Vega IE, Mufson EJ. Biomarkers for the early detection and progression of Alzheimer's disease. *Neurotherapeutics.* 2017;14:35–53.
64. Penke B, Bogar F, Fulop L. Beta-amyloid and the pathomechanisms of Alzheimer's disease: a comprehensive view. *Molecules.* 2017;22(10):1692. <https://doi.org/10.3390/molecules22101692>.
65. Acharya MM, Christie LA, Lan ML, Giedzinski E, Fike JR, Rosi S, Limoli CL. Human neural stem cell transplantation ameliorates radiation-induced cognitive dysfunction. *Cancer Res.* 2011;71:4834–45.
66. Acharya MM, Martirosian V, Chmielewski NN, Hanna N, Tran KK, Liao AC, Christie LA, Parihar VK, Limoli CL. Stem cell transplantation reverses chemotherapy-induced cognitive dysfunction. *Cancer Res.* 2015;75:676–86.
67. Rajendran L, Paolicelli RC. Microglia-mediated synapse loss in Alzheimer's disease. *J Neurosci.* 2018;38:2911–9.
68. Shi Q, Chowdhury S, Ma R, Le KX, Hong S, Caldaroni BJ, Stevens B, Lemere CA. Complement C3 deficiency protects against neurodegeneration in aged plaque-rich APP/PS1 mice. *Sci Transl Med.* 2017;9(392):eaaf6295. <https://doi.org/10.1126/scitranslmed.aaf6295>.
69. Sommer A, Marxreiter F, Krach F, Fadler T, Grosch J, Maroni M, Graef D, Eberhardt E, Riemenschneider MJ, Yeo GW, et al. Th17 lymphocytes induce neuronal cell death in a human iPSC-based model of Parkinson's disease. *Cell Stem Cell.* 2018;23:123–31 e126.

## Publisher's Note

Springer Nature remains neutral with regard to jurisdictional claims in published maps and institutional affiliations.